Metascatter: Unifying Symbiotic Radio and Intelligent Reflecting Surface

Yang Zhao, *Member, IEEE,* and Bruno Clerckx, *Fellow, IEEE*

***Abstract*—Backscatter nodes can harvest energy from, modulate information over, and reconfigure propagation of ambient signals. We uniquely introduce *Metascatter* that adapts the input distribution of a finite-state passive backscatter node based on Channel State Information (CSI), to *simultaneously* encode self message and assist legacy transmission while powered by surrounding waves. Compared to existing Intelligent Reflecting Surface (IRS)-empowered Symbiotic Radio (SR) that encodes and precodes independently using advanced architecture (e.g., overlay or parallel), Metascatter softly bridges and generalizes parasitic source of SR and reflecting element of IRS via smart input design. This not only reduces hardware complexity and optimization cost, but also enables a flexible tradeoff between primary (legacy) and backscatter links using shared spectrum, energy, and infrastructures. Moreover, we consider a specific scenario where a multi-antenna Access Point (AP) serves a single-antenna user surrounded by multiple Metascatters. For simplicity, it is assumed the user first jointly decodes all backscatter messages based on average received power, then models reflection patterns and backscatter paths within equivalent channel for primary decoding. We characterize the achievable primary-(total-)backscatter rate region by optimizing the input distribution at Metascatters, the active beamforming at the AP, and the decision regions at the user. A suboptimal Block Coordinate Descent (BCD) algorithm is proposed, where the Karush–Kuhn–Tucker (KKT) input distribution is evaluated in closed form, the active beamforming is updated by Projected Gradient Descent (PGD), and the suboptimal convex decision regions are refined by Dynamic Programming (DP). Simulation results demonstrate Metascatters can exploit additional propagation paths to transmit and assist via input design.**

I. Introduction

BACKSCATTER is recently re-innovated as a promising approach to support low-power communications and control wireless propagation environments. Ambient Backscatter Communications (AmBC) that enables battery-free communication between interactive nodes was first introduced and prototyped in [1], where devices harvest energy from and modulate information over ambient Radio-Frequency (RF) signals by switching between reflecting and absorbing states. To combat the strong direct-link interference of AmBC, [2] exploited the repeating structure of Orthogonal Frequency-Division Multiplexing (OFDM) symbol and proposed a multi-antenna detector that only requires the backscatter channel strength. Cooperative AmBC that decodes primary and backscatter links using co-located receiver was proposed in [3], where the authors evaluated the error performance of Maximum-Likelihood (ML), linear, and Successive Interference Cancellation (SIC) detectors for flat fading channels and proposed a low-complexity ML detector for frequency-selective fading channels. The concept was then generalized to SR in [4] to "exploit the benefits and address the drawbacks" of Cognitive Radio (CR) and AmBC. The authors of [5] classified SR into commensal, parasitic, and competitive types based on link priority, and derived their instantaneous rates and optimal power allocations. The corresponding outage probabilities were also studied in [6]. Besides, [7] concluded that if the backscatter symbol period is sufficiently long, then the non-coherent primary rate would approach its coherent counterpart. The authors thus proposed to decode the primary link under backscatter uncertainty, then perform SIC and decode the backscatter link. [8] also explored the asymptotic impact of transmit/receive antenna and backscatter symbol period on the ergodic rate of primary and backscatter links. For a Multiple-Input Multiple-Output (MIMO) SR system with a multi-antenna backscatter node, [9] proposed a beamforming design to maximize the backscatter rate while guaranteeing the primary performance. However, those paper only considered one backscatter node and backscatter multiple access remains an open issue. In [10], a Non-Orthogonal Multiple Access (NOMA)-based SR was proposed and receive combining was investigated when SIC order follows equivalent channel strength. A Time-Division Multiple Access (TDMA)-based SR with energy harvesting constraints was also presented in [11], where transmit power, reflection efficiency, and time allocation were jointly optimized to maximize energy efficiency. To reduce coordination between passive nodes, [12] proposed a random code-assisted multiple access for SR and evaluated the asymptotic Signal-to-Interference-plus-Noise Ratio (SINR) using random matrix theory.

On the other hand, IRS alters propagation environment for legacy networks using numerous sub-wavelength passive elements with adaptive amplitudes and/or phases. Extensive research has been devoted to optimizing the phase shifts for the whole channel block to improve communication, sensing, and power performances [13]–[18]. Besides, [19] proposed a dynamic passive beamforming that further adjusts IRS over fine-grained time slots for OFDM systems to balance beamforming gain and multiuser diversity. The idea was further applied to Wireless Powered Communication Network (WPCN) to accommodate the downlink Wireless Power Transfer (WPT) phase and uplink Wireless Information Transfer (WIT) phase of the "harvest-then-transmit" protocol [20], [21]. For multiuser WPT, [22] also reported that dynamic beamforming can mimic multi-beam reflection in a time-division manner and reduce the phase extraction loss. Although dynamic passive beamforming artificially creates temporal diversity for flexible channel

The authors are with the Department of Electrical and Electronic Engineering, Imperial College London, London SW7 2AZ, U.K. (e-mail: {yang.zhao18, b.clerckx}@imperial.ac.uk).

reconfiguration and resource allocation, it demands additional computational cost and control overhead, and the tradeoff deserves further attention especially for large IRS. In [23], [24], IRS was also introduced to single- and multi-node SR systems to reduce the total transmit power. When joint transmitter-IRS encoding is possible, [25] proved using IRS only for passive beamforming is generally suboptimal in terms of achievable rate for finite input constellations. Recently, IRS-empowered SR was introduced in [26]–[28] where independent passive beamforming and backscatter encoding were combined using advanced architectures. The authors of [26], [27] proposed the IRS to modulate binary message over the whole phase shift matrix and the receiver to decodes from (non-coherent) primary to (coherent) backscatter link. In contrast, [28] divided the IRS into reflection and information elements, and evaluated the error performance of non-coherent backscatter detection.

To the best of our knowledge, most existing SR systems [3], [5]–[10] assumed Gaussian codebook at backscatter nodes, and considered SIC from primary to backscatter link. It thus requires non-coherent encoding at the transmitter and re-encoding, precoding, and subtraction processes at the receiver. Besides, the advantage of SIC is questionable because 1) the primary and backscatter symbols are mixed by multiplication instead of superposition, and 2) the backscatter symbol period is typically much longer under physical constraints. Motivated by those, we introduce Metascatter that adapts the input distribution of a finite-state passive backscatter node based on CSI to unify backscatter sources of SR and reflecting elements of IRS. An application scenario was considered where multiple Metascatters ride over a point-to-point transmission to simultaneously encode self message and perform passive beamforming. To fully accommodate backscatter characteristics, we also propose a novel receiving strategy that first jointly decodes all Metascatter based on average received power, then models their reflection patterns and backscatter paths within equivalent channel for primary decoding. The contributions of this paper is summarized as follows.

First, Metascatter adapts the input probability distribution of a finite-state backscatter device based on the primary and backscatter CSI. It generalizes the backscatter tags of SR and reflecting elements of IRS to improve the primary-backscatter tradeoff in a flexible manner. When the primary link is absolutely prioritized, the tag input probability boils down to 1 at the state that maximizes the equivalent channel strength and 0 at other states, which is essentially the phase shift selection of an IRS element. When we only care about the backscatter performance, the network boils down to a multi-tag AmBC and the input design can be simplified accordingly.

Second, we propose a novel receiving strategy where the backscatter symbol of all tags are first recovered by energy-based decoding, then modeled within equivalent CSI for primary decoding. When the ratio of backscatter symbol period over primary symbol period is large enough, the randomness of primary source can be averaged out and the performance of non-coherent backscatter decoding can be greatly improved. Since the primary and backscatter symbols are mixed by multiplication coding, the backscatter decoding can be viewed as part of primary channel training, which avoids non-coherent encoding at the transmitter and SIC at the receiver.

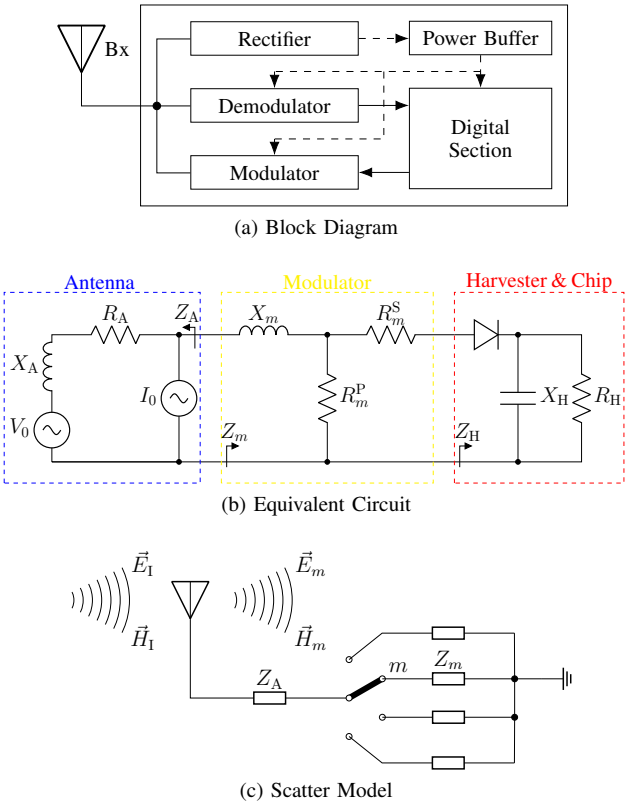

Fig. 1. Block diagram, equivalent circuit, and scatter model of a typical passive tag. The solid and dashed vectors represent signal and energy flows. The backscatter antenna behaves as a constant power source, where the voltage V_0 and current I_0 are introduced by incident electric field $\vec{E}_{\rm I}$ and magnetic field $\vec{H}_{\rm I}$ [29].

Third, we characterize the achievable primary-(total-)backscatter rate region by iteratively optimizing the tag input distribution, the backscatter decision threshold, and the transmit precoder. For the input design, we propose a numerical method to evaluate the KKT solutions by limits of sequences. For the threshold design, we derive the minimum number of decision thresholds to maximize the total backscatter rate, and obtain the optimal thresholds by DP accelerated by Shor-Moran-Aggarwal-Wilber-Klawe (SMAWK) algorithm. However, the optimal precoder design can be non-trivial and we may end up with a low-complexity suboptimal solution.

II. Backscatter Principles

Passive backscatter devices (a.k.a., tags) harvest energy from and modulate information over surrounding RF signal. As shown in Fig. 1(a), a typical passive tag consists of a scattering antenna, an energy harvester, an integrated receiver, a load-switching modulator, and on-chip components (e.g., micro-controller and sensors) [30]. Its equivalent circuit is also given by Fig. 1(b). When illuminated, the tag absorbs a portion of the impinging wave and scatters the rest back to the space. The absorbed signal can be used for source decoding and energy harvesting [31], while the scattered signal can be decomposed into the *structural* and *antenna* mode components [32]. The structural mode scattering applies to general objects and is related

to the antenna structure, shape and material, which contributes to environment multipath and can be covered by channel estimation [33]. On the other hand, the antenna mode scattering models the antenna radiation and depends on the antenna-load impedance mismatch, which can be used for backscatter modulation [34] or channel reconfiguration [35]. Fig. 1(c) illustrates the scatter model. For a tag with M candidate states, the reflection coefficient of state $m \in \mathcal{M} \triangleq \{1,...,M\}$ is defined as [1]t corresponds to a linear backscatter model where the reflection coefficient is irrelevant to incident electromagnetic field strength.

$$\Gamma_m = \frac{Z_m - Z_{\mathrm{A}}^*}{Z_m + Z_{\mathrm{A}}}, \tag{1}$$

where Z_m is the load impedance at state m and Z_{A} is the antenna input impedance.

A. Backscatter Modulation

In backscatter modulation, the tag *periodically varies* the reflection coefficient to embed its own information. As such, there exists a mapping from the alphabet to the set. When the CSI and reflection alphabet $\{\Gamma_1,...,\Gamma_M\}$ are available at the reader, it can decode the tag message from the observed scattered signal.

For M-ary Quadrature Amplitude Modulation (QAM), the complex constellation point c_m maps to the corresponding reflection coefficient by [36]

$$\Gamma_m = \alpha \frac{c_m}{\max_{m'} |c_{m'}|}, \tag{2}$$

where $\alpha \in [0,1]$ models the amplitude scatter ratio at the direction of interest.

B. Channel Reconfiguration

2 For passive tags, $\alpha \ll 1$ is commonly assumed as the majority of the incident wave can be harvested to support tag modules [36].

Remark 1. *By choosing proper load impedance, it is possible to implement any signal constellation or think beyond modulation. For example, perfect matching enables maximum power transfer to the tag, while perfect mismatch leads to complete reflection as desired by ideal IRS. It inspires Metascatter to design a smart reflection and unify wireless power transfer, backscatter modulation, and passive beamforming.*

III. Metascatter

A. System Model

As shown in Fig. 3, we propose a single-user (UE) multi-tag (TG) symbiotic radio network where the RF signal generated by the Q-antenna AP is shared by two coexisting systems. In the primary point-to-point system, the AP transmits information to the single-antenna user. In the secondary backscatter system, the AP acts as the carrier emitter, the K nearby single-antenna tags modulate their information over the reradiated RF signals, and the user receives and decodes the backscatter messages. Denote the AP-UE direct channel as $\boldsymbol{h}_{\mathrm{D}}^H \in \mathbb{C}^{1\times Q}$, the AP-TG $k \in \mathcal{K} \triangleq \{1,\dots,K\}$ forward channel as $\boldsymbol{h}_{\mathrm{F},k}^H \in \mathbb{C}^{1\times Q}$, the TG k-UE

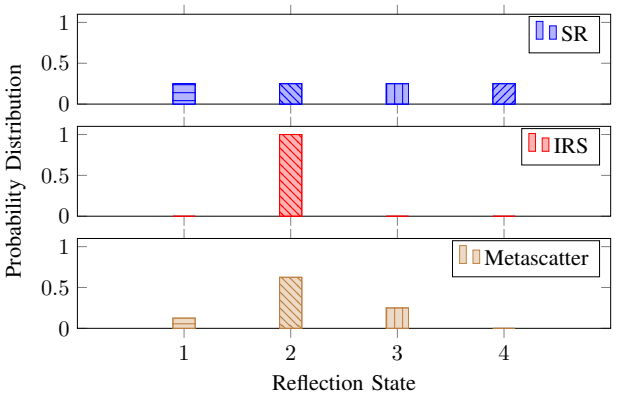

(a) Reflection State Distribution

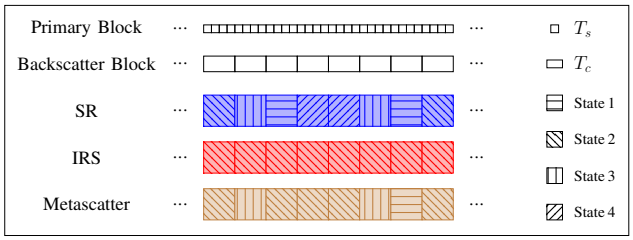

(b) Time Block Structure

Fig. 2. Reflection state distribution and time block structure of SR, IRS, and Metascatter. T_s and T_c denote the primary and backscatter symbol length, respectively. Based on CSI, Metascatter adapts the reflection state distribution to unify data transmission and channel reconfiguration.

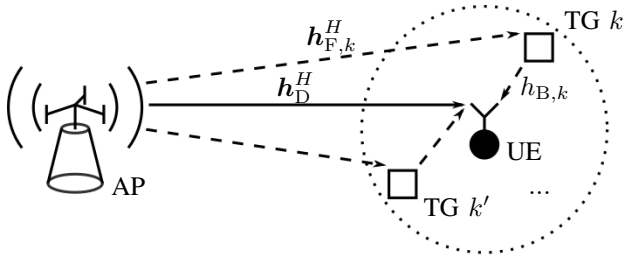

Fig. 3. The proposed Metascatter system.

backward channel as $h_{\mathrm{B},k}$, and define the cascaded channel of tag k as $\boldsymbol{h}_{\mathrm{C},k}^H \triangleq h_{\mathrm{B},k} \boldsymbol{h}_{\mathrm{F},k}^H \in \mathbb{C}^{1\times Q}$. For simplicity, we consider a quasi-static block fading model where the channel response remain constant within each coherence interval and vary independently between consecutive blocks. Since backscatter modulation involves load switching, tags typically transmit at much lower rate, and we assume the backscatter symbol length is $N \in \mathbb{Z}_{++}$ times the primary symbol length. We also assume the direct channel and all cascaded channels can be estimated and fed back to the AP. [2]ue to the lack of RF chains at the passive tag, accurate and efficient CSI acquisition at the AP can be challenging. One possible approach is that the AP sends pre-defined pilots, the tags respond in well-designed manners, and the user performs least-square estimation with feedbacks [37]–[39].

Consider the signal model during one backscatter symbol period. We assume the primary symbol follows standard Circularly Symmetric Complex Gaussian (CSCG) distribution and the backscatter symbol of all tags employs M-QAM.

[1]I

[2]D

Under perfect synchronization, the signal received by the user at primary symbol block $n \in \mathcal{N} \triangleq \{1,...,N\}$ is [3]e omit the signal reflected by two or more times [40] and assume the time difference of arrival from different paths are negligible [5].

$$y[n] = \left(\boldsymbol{h}_{\mathrm{D}}^H + \sum_{k \in \mathcal{K}} \sqrt{\alpha_k} \boldsymbol{h}_{\mathrm{C},k}^H x_k \right) \boldsymbol{w} s[n] + w[n], \tag{3}$$

where α_k and x_k denote respectively the harvest-backscatter efficiency and backscatter symbol of tag k, $s[n]$ and $w[n] \sim \mathcal{CN}(0, \sigma_w^2)$ denote respectively the primary symbol and Additive White Gaussian Noise (AWGN) at block n, and $\boldsymbol{w} \in \mathbb{C}^{Q \times 1}$ is the transmit precoder satisfying power constraint $\|\boldsymbol{w}\|^2 \leq P$. For the ease of notation, we define $x_{\mathcal{K}} \triangleq \{x_k : k \in \mathcal{K}\}$ as the tag input combination, and $\boldsymbol{y} \triangleq [y[1],...,y[N]]^T \in \mathbb{C}^{N \times 1}$ as the received signal per backscatter symbol period. For primary transmission, the equivalent channel is subject to backscatter modulation uncertainty as

$$\boldsymbol{h}_{\mathrm{E}}^H(x_{\mathcal{K}}) \triangleq \boldsymbol{h}_{\mathrm{D}}^H + \sum_{k \in \mathcal{K}} \sqrt{\alpha_k} \boldsymbol{h}_{\mathrm{C},k}^H x_k. \tag{4}$$

Remark 2. *Metascatter involves an unconventional Multiple Access Channel (MAC) where the primary and backscatter symbols of different duration are mixed by Multiplication Coding (MC) instead of Superposition Coding (SC). For each tag, the reflection coefficient not only encodes the backscatter message but also influences the equivalent primary channel* (4)*. As such, novel receiving strategy other than SIC should be tailored to signal characteristics to unveil how reflection pattern potentially influences the primary-backscatter tradeoff.*

B. Receiving Strategy

We propose a novel receiving strategy where the backscatter symbol of all tags are first jointly identified by non-coherent energy detection, then modeled within equivalent channel (4) as if passive beamforming. Compared with conventional schemes as joint decoding and SIC, the Metascatter receiver may not achieve as high data rate for one tag, but it avoids non-coherent primary encoding and enables tag multiple access in a practical and low-complexity manner. Therefore, we believe it can be compatible to and readily implemented over legacy point-to-point systems.

Define $m_k \in \mathcal{M}$ as the modulation index of tag k, and $m_{\mathcal{K}} \triangleq \{m_k : k \in \mathcal{K}\}$ as the modulation index combination of all tags. Recall that x_k and $x_{\mathcal{K}}$ are random variables representing the backscatter symbol of tag k and the symbol combination of all tags, respectively. Their instances are denoted by modulation index (combination) as x_{m_k} and $x_{m_{\mathcal{K}}}$. Since any backscatter combination $x_{m_{\mathcal{K}}}$ remains unchanged over N primary symbol duration, the received signal at symbol block n is only subject to the variation of $s[n]$ and $w[n]$, and follows zero-mean CSCG distribution with variance

$$\sigma_{m_{\mathcal{K}}}^2 = \Bigg| \underbrace{\left(\boldsymbol{h}_{\mathrm{D}}^H + \sum_{k \in \mathcal{K}} \sqrt{\alpha_k} \boldsymbol{h}_{\mathrm{C},k}^H x_{m_k} \right)}_{\boldsymbol{h}_{\mathrm{E}}^H(x_{m_{\mathcal{K}}})} \boldsymbol{w} \Bigg|^2 + \sigma_w^2. \tag{5}$$

[3]W

Besides, we denote the total received energy as $z \triangleq \|\boldsymbol{y}\|^2$ and the hypothesis of modulation index combination $m_{\mathcal{K}}$ as $\mathcal{H}_{m_{\mathcal{K}}}$. Since z is the sum of N independent and identically distributed (i.i.d.) exponential variables, its conditional Probability Density Function (PDF) under $\mathcal{H}_{m_{\mathcal{K}}}$ follows Erlang distribution with shape N and scale $\sigma_{m_{\mathcal{K}}}^2$ as

$$f(z \,|\, \mathcal{H}_{m_{\mathcal{K}}}) = \frac{z^{N-1} e^{-z/\sigma_{m_{\mathcal{K}}}^2}}{\sigma_{m_{\mathcal{K}}}^{2N} (N-1)!}. \tag{6}$$

Energy-based backscatter detection essentially formulates a discrete-input continuous-output memoryless MAC. To further reduce decoding complexity, we divide the continuous output z into disjoint decision regions to construct a Discrete Memoryless Thresholding Multiple Access Channel (DMTMAC), where the transition probability from tag input combination $x_{m_{\mathcal{K}}}$ to detector output combination $\hat{x}_{m'_{\mathcal{K}}}$ is

$$P(\hat{x}_{m'_{\mathcal{K}}} \,|\, x_{m_{\mathcal{K}}}) = \int_{\mathcal{R}_{m'_{\mathcal{K}}}} f(z \,|\, \mathcal{H}_{m_{\mathcal{K}}}) \mathrm{d}z, \tag{7}$$

where $\mathcal{R}_{m'_{\mathcal{K}}}$ is the decision region over z for hypothesis $\mathcal{H}_{m'_{\mathcal{K}}}$.

C. Achievable Rates

Denote the input probability distribution vector of tag k as $\boldsymbol{p}_k \triangleq [P_k(x_1),...,P_k(x_M)]^T \in \mathbb{R}^{M \times 1}$, where $P_k(x_{m_k})$ is the probability at state m_k. Consider independent encoding at all tags such that the probability of input combination $x_{m_{\mathcal{K}}}$ is $P_{\mathcal{K}}(x_{m_{\mathcal{K}}}) = \prod_{k \in \mathcal{K}} P_k(x_{m_k})$. The backscatter information function of input combination $x_{m_{\mathcal{K}}}$ is defined as

$$I_{\mathrm{B}}(x_{m_{\mathcal{K}}}; \hat{x}_{\mathcal{K}}) \triangleq \sum_{m'_{\mathcal{K}}} P(\hat{x}_{m'_{\mathcal{K}}} \,|\, x_{m_{\mathcal{K}}}) \log \frac{P(\hat{x}_{m'_{\mathcal{K}}} \,|\, x_{m_{\mathcal{K}}})}{P(\hat{x}_{m'_{\mathcal{K}}})}, \tag{8}$$

where $P(\hat{x}_{m'_{\mathcal{K}}}) = \sum_{m_{\mathcal{K}}} P_{\mathcal{K}}(x_{m_{\mathcal{K}}}) P(\hat{x}_{m'_{\mathcal{K}}} \,|\, x_{m_{\mathcal{K}}})$. Besides, the backscatter marginal information function associated with letter x_{m_k} of tag k is

$$I_{\mathrm{B},k}(x_{m_k}; \hat{x}_{\mathcal{K}}) \triangleq \sum_{m_{\mathcal{K} \setminus \{k\}}} P_{\mathcal{K} \setminus \{k\}}(x_{m_{\mathcal{K} \setminus \{k\}}}) I_{\mathrm{B}}(x_{m_{\mathcal{K}}}; \hat{x}_{\mathcal{K}}), \tag{9}$$

where $P_{\mathcal{K} \setminus \{k\}}(x_{m_{\mathcal{K} \setminus \{k\}}}) = \prod_{q \in \mathcal{K} \setminus \{k\}} P_q(x_{m_q})$. Therefore, the backscatter mutual information is

$$I_{\mathrm{B}}(x_{\mathcal{K}}; \hat{x}_{\mathcal{K}}) = \sum_{m_{\mathcal{K}}} P_{\mathcal{K}}(x_{m_{\mathcal{K}}}) \sum_{m'_{\mathcal{K}}} P(\hat{x}_{m'_{\mathcal{K}}} \,|\, x_{m_{\mathcal{K}}}) \log \frac{P(\hat{x}_{m'_{\mathcal{K}}} \,|\, x_{m_{\mathcal{K}}})}{P(\hat{x}_{m'_{\mathcal{K}}})}. \tag{10}$$

Once the tag input combination is successfully decoded, the backscatter uncertainty can be eliminated and the equivalent channel for primary transmission can be updated by (4). Similar to above, the primary information function of input combination $x_{m_{\mathcal{K}}}$ is

$$I_{\mathrm{P}}(x_{m_{\mathcal{K}}}; \boldsymbol{y}) \triangleq \log_2 \left(1 + \frac{|\boldsymbol{h}_{\mathrm{E}}^H(x_{m_{\mathcal{K}}}) \boldsymbol{w}|^2}{\sigma_w^2} \right), \tag{11}$$

the primary marginal information function associated with letter x_{m_k} of tag k is

$$I_{\mathrm{P},k}(x_{m_k}; \boldsymbol{y}) \triangleq \sum_{m_{\mathcal{K} \setminus \{k\}}} P_{\mathcal{K} \setminus \{k\}}(x_{m_{\mathcal{K} \setminus \{k\}}}) I_{\mathrm{P}}(x_{m_{\mathcal{K}}}; \boldsymbol{y}), \tag{12}$$

and the primary (ergodic) mutual information is

$$I_{\mathrm{P}}(x_{\mathcal{K}};\boldsymbol{y})=\sum_{m_{\mathcal{K}}}P_{\mathcal{K}}(x_{m_{\mathcal{K}}})\log_2\left(1+\frac{|\boldsymbol{h}_{\mathrm{E}}^H(x_{m_{\mathcal{K}}})\boldsymbol{w}|^2}{\sigma_w^2}\right). \quad (13)$$

Therefore, the weighted sum information function, marginal information function, and mutual information of primary and backscatter links are respectively given by

$$I(x_{m_{\mathcal{K}}};\hat{x}_{\mathcal{K}},\boldsymbol{y})\triangleq\rho I_{\mathrm{P}}(x_{m_{\mathcal{K}}};\boldsymbol{y})+(1-\rho)I_{\mathrm{B}}(x_{m_{\mathcal{K}}};\hat{x}_{\mathcal{K}}), \quad (14)$$

$$I_k(x_{m_k};\hat{x}_{\mathcal{K}},\boldsymbol{y})\triangleq\rho I_{\mathrm{P},k}(x_{m_k};\boldsymbol{y})+(1-\rho)I_{\mathrm{B},k}(x_{m_k};\hat{x}_{\mathcal{K}}), \quad (15)$$

$$I(x_{\mathcal{K}};\hat{x}_{\mathcal{K}},\boldsymbol{y})\triangleq\rho I_{\mathrm{P}}(x_{\mathcal{K}};\boldsymbol{y})+(1-\rho)I_{\mathrm{B}}(x_{\mathcal{K}};\hat{x}_{\mathcal{K}}), \quad (16)$$

where $\rho\in[0,1]$ represents the priority of the primary link.

IV. Input, Threshold, and Precoder Design

To characterize the achievable primary-(total-)backscatter rate region of Metascatter, we aim to maximize the weighted sum mutual information with respect to tag input probability distribution $\{\boldsymbol{p}_k\}$, decision threshold vector $\boldsymbol{t}$, and transmit precoder $\boldsymbol{w}$

$$\max_{\{\boldsymbol{p}_k\},\boldsymbol{t},\boldsymbol{w}} \quad I(x_{\mathcal{K}};\hat{x}_{\mathcal{K}},\boldsymbol{y}) \quad (17a)$$

$$\text{s.t.} \quad \sum\nolimits_{m_k}P_k(x_{m_k})=1, \quad \forall k\in\mathcal{K}, \quad (17b)$$

$$P_k(x_{m_k})\geq 0, \quad \forall k\in\mathcal{K},\ \forall m_k\in\mathcal{M}, \quad (17c)$$

$$\|\boldsymbol{w}\|^2\leq P. \quad (17d)$$

Since problem (17) is not jointly convex, we propose a BCD algorithm that iteratively updates $\{\boldsymbol{p}_k\}$, $\boldsymbol{t}$ and $\boldsymbol{w}$ until convergence.

A. Input Probability Distribution

For any fixed decision boundary $\boldsymbol{t}$ and transmit precoder $\boldsymbol{w}$, the equivalent DMTMAC can be formulated by (7) and problem (17) boils down to

$$\max_{\{\boldsymbol{p}_k\}} \quad I(x_{\mathcal{K}};\hat{x}_{\mathcal{K}},\boldsymbol{y}) \quad (18a)$$

$$\text{s.t.} \quad \text{(17b),(17c)}, \quad (18b)$$

which involves the product term $\prod_{k\in\mathcal{K}}P_k(x_{m_k})$ and is non-convex when $K>1$. Interestingly, the total-rate optimal input design for general discrete memoryless MAC remains an open problem, and we instead propose a KKT solution to problem (18). [4]s pointed out in [41], KKT conditions are only necessary for total-rate optimality and these solutions may end up being saddle points.

Proposition 1. *The KKT optimality conditions for problem* (18) *are equivalent to,* $\forall k\in\mathcal{K}$ *and* $\forall m_k\in\mathcal{M}$*,*

$$I_k^\star(x_{m_k};\hat{x}_{\mathcal{K}},\boldsymbol{y})=I^\star(x_{\mathcal{K}};\hat{x}_{\mathcal{K}},\boldsymbol{y}), \quad P_k^\star(x_{m_k})>0, \quad (19a)$$

$$I_k^\star(x_{m_k};\hat{x}_{\mathcal{K}},\boldsymbol{y})\leq I^\star(x_{\mathcal{K}};\hat{x}_{\mathcal{K}},\boldsymbol{y}), \quad P_k^\star(x_{m_k})=0. \quad (19b)$$

Proof. Please refer to Appendix A. □

[4]A

We notice (19a) means each probable state of each tag should produce the same marginal information (averaged over all states of other tags), while (19b) implies any state of any tag with potentially less marginal information than above should not be used. Next, we generalize the Blahut-Arimoto algorithm [42], [43] and propose a numerical evaluation of KKT points by limits of sequences.

Proposition 2. *The KKT solution of input probability of tag* k *at state* m_k *is given by the converging point of the sequence*

$$P_k^{(r+1)}(x_{m_k})=\frac{P_k^{(r)}(x_{m_k})\exp\left(\frac{\rho}{1-\rho}I_k^{(r)}(x_{m_k};\hat{x}_{\mathcal{K}},\boldsymbol{y})\right)}{\sum_{m_k'}P_k^{(r)}(x_{m_k'})\exp\left(\frac{\rho}{1-\rho}I_k^{(r)}(x_{m_k'};\hat{x}_{\mathcal{K}},\boldsymbol{y})\right)}, \quad (20)$$

where r *is the iteration index and* $\boldsymbol{p}_k^{(0)}>\boldsymbol{0}$*,* $\forall k\in\mathcal{K}$*. At each iteration, the input distribution of tag* k *is evaluated based on the updated input distribution of tags* 1 *to* $k-1$*.*

Proof. Please refer to Appendix B. □

B. Decision Threshold

For a given tag input distribution $\{\boldsymbol{p}_k\}$, we can formulate an equivalent information source with augmented alphabet of tag input combination. This equivalent source transmits at the total backscatter rate, and the input distribution is given by $P_{\mathcal{K}}(x_{m_{\mathcal{K}}})=\prod_{k\in\mathcal{K}}P_k(x_{m_k})$, $\forall k\in\mathcal{K}$ and $\forall m_k\in\mathcal{M}$.

Remark 3. *Since the equivalent source transmits at the total backscatter rate, the DMTMAC* (7) *is essentially a point-to-point Discrete Memoryless Thresholding Channel (DMTC) and we can simplify the decision threshold design accordingly.*

Interestingly, the optimal threshold design to maximize the mutual information for a general DMTC with a fixed number of output letters remains an open issue. The reason is that each decision region may contain more than one disjoint partitions (i.e., non-convex) and the number of thresholds are unknown. Fortunately, for the proposed energy detection, we proved that the DMTC capacity can be achieved using only convex decision regions. This conclusion is summarized below.

Proposition 3. *For a discrete-input continuous-output channel in Erlang distribution* (6)*, if the DMTC is constructed for detection (i.e., same input/output alphabet) and* L *input letters are with non-zero probability, then it is possible to achieve the DMTC capacity by* L *non-empty convex decision regions defined by* $L+1$ *distinct decision thresholds.*

Proof. Please refer to Appendix C. □

Once the optimal number of decision threshold is determined, we can first discretize the output energy level into numerous bins, then obtain the optimal decision regions that maximizes the total backscatter rate by DP accelerated by SMAWK algorithm [44].

We may need to tailor threshold design for Metascatter as threshold design has potential impact on primary achievable rate, as implied by some simulation results.

TABLE I
PARAMETERS IN SIMULATION

Transmit antenna Q	1
Tags K	2
States M	2
Reflect ratio α	0.5
Duration ratio N	10
Noise power σ_w^2	1
Discretization bins	256

C. Precoder

The optimal precoder design is highly non-convex that involves integration, entropy term, and variable on exponential. We may propose a suboptimal precoder based on linear combination of equivalent and cascaded channels, or consider single transmit antenna instead.

$$I(x_i;\hat{x}_j)=\sum_{j\in\mathcal{I}}\int_{t_{j-1,j}}^{t_{j,j+1}}\frac{z^{N-1}\exp\left(-\frac{z}{\mathrm{tr}(H_{\mathrm{E},i}W)+\sigma_w^2}\right)}{(\mathrm{tr}(H_{\mathrm{E},i}W)+\sigma_w^2)^N(N-1)!}\mathrm{d}z \times\log\frac{\int_{t_{j-1,j}}^{t_{j,j+1}}\frac{z^{N-1}\exp\left(-\frac{z}{\mathrm{tr}(H_{\mathrm{E},i}W)+\sigma_w^2}\right)}{(\mathrm{tr}(H_{\mathrm{E},i}W)+\sigma_w^2)^N(N-1)!}\mathrm{d}z}{\sum_{i'\in\mathcal{I}}\int_{t_{j-1,j}}^{t_{j,j+1}}\frac{z^{N-1}\exp\left(-\frac{z}{\mathrm{tr}(H_{\mathrm{E},i'}W)+\sigma_w^2}\right)}{(\mathrm{tr}(H_{\mathrm{E},i'}W)+\sigma_w^2)^N(N-1)!}\mathrm{d}z}, \tag{21}$$

V. Preliminary Results

Table I shows the parameters used in simulation. We assume all links are in standard CSCG distribution and evaluated the rate regions on two instances. For the input design, "Cooperation" assumes full transmit cooperation at all tags (i.e., joint encoding), "Exhaustion" runs exhaustive search on all possible input distributions, "KKT" is proposed KKT input design (20), and "Marginalization" marginalizes the joint input array by "Cooperation" to obtain independent tag input distribution. For the threshold design, "SMAWK" refers to the DP-based quantization proposed in [44], "Bisection" sequentially optimizes each threshold by bisection [45], and "ML" is the ML detector that requires no knowledge of input distribution.

Figs. 4 and 5 show two typical scenarios where joint encoding can be helpful and unnecessary, respectively. Although the proposed KKT input design converges to the optimal solutions in both examples, it may be trapped at saddle points under poor initialization, especially when the number of tags increases.

We believed threshold design has no impact on the primary achievable rate, because primary decoding acts on $\boldsymbol{y}$ while thresholding acts on z. As such, the threshold that maximizes the total backscatter rate should also maximize the weighted sum rate. Interestingly, this may not be the case because the SMAWK and Bisection threshold designs, both maximizing the total backscatter rate, can be outperformed by the ML when it comes to weighted sum primary-(total-)backscatter rate. It may result from a precision issue, but inspires further research on threshold design for Metascatter.

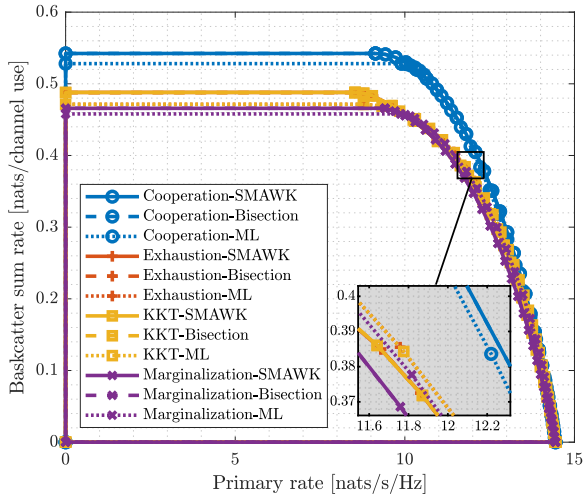

Fig. 4. Achievable rate regions by input-threshold design: Case I.

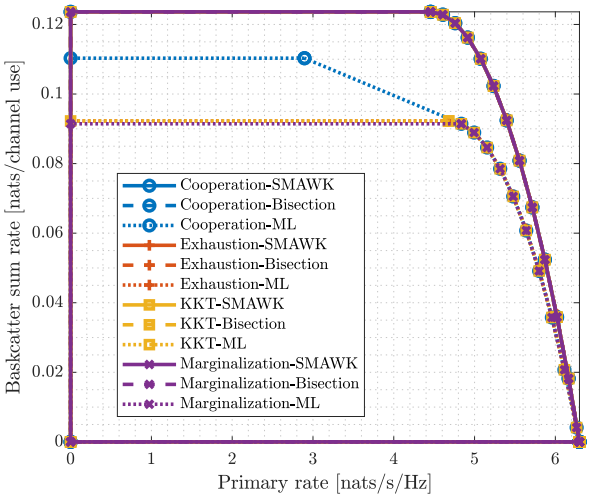

Fig. 5. Achievable rate regions by input-threshold design: Case II.

Appendix

A. Proof of Proposition 1

Denote the Lagrange multipliers associated with (17b) and (17c) as $\{\nu_k\}_{k\in\mathcal{K}}$ and $\{\lambda_{k,m_k}\}_{k\in\mathcal{K},m_k\in\mathcal{M}}$, respectively. The Lagrangian function of problem (18) is

$$L=-I(x_{\mathcal{K}};\hat{x}_{\mathcal{K}},\boldsymbol{y})+\sum_{k\in\mathcal{K}}\nu_k\left(\sum_{m_k\in\mathcal{M}}P_k(x_{m_k})-1\right) -\sum_{k\in\mathcal{K}}\sum_{m_k\in\mathcal{M}}\lambda_{k,m_k}P_k(x_{m_k}), \tag{22}$$

and the KKT conditions on the optimal primal and dual variables are, $\forall m_k\in\mathcal{M}$ and $\forall k\in\mathcal{K}$,

$$-\nabla_{P_k^\star(x_{m_k})}I^\star(x_{\mathcal{K}};\hat{x}_{\mathcal{K}},\boldsymbol{y})+\nu_k^\star-\lambda_{k,m_k}^\star=0, \tag{23a}$$

$$\lambda_{k,m_k}^\star=0,\quad P_k^\star(x_{m_k})>0, \tag{23b}$$

$$\lambda_{k,m_k}^\star\geq 0,\quad P_k^\star(x_{m_k})=0, \tag{23c}$$

where the directional derivative can be explicitly expressed as

$$\nabla_{P_k^\star(x_{m_k})} I^\star(x_{\mathcal{K}};\hat{x}_{\mathcal{K}},\boldsymbol{y}) = I_k^\star(x_{m_k};\hat{x}_{\mathcal{K}},\boldsymbol{y}) - (1-\rho). \tag{24}$$

Combining (23) and (24), we have

$$I_k^\star(x_{m_k};\hat{x}_{\mathcal{K}},\boldsymbol{y}) = \nu_k^\star + (1-\rho), \quad P_k^\star(x_{m_k}) > 0, \tag{25a}$$
$$I_k^\star(x_{m_k};\hat{x}_{\mathcal{K}},\boldsymbol{y}) \le \nu_k^\star + (1-\rho), \quad P_k^\star(x_{m_k}) = 0, \tag{25b}$$

which suggests

$$\sum_{m_k} P_k^\star(x_{m_k}) I_k^\star(x_{m_k};\hat{x}_{\mathcal{K}},\boldsymbol{y}) = \nu_k^\star + (1-\rho). \tag{26}$$

On the other hand, by definition of weighted sum marginal information (15),

$$\sum_{m_k} P_k^\star(x_{m_k}) I_k^\star(x_{m_k};\hat{x}_{\mathcal{K}},\boldsymbol{y}) = I^\star(x_{\mathcal{K}};\hat{x}_{\mathcal{K}},\boldsymbol{y}), \tag{27}$$

where the right-hand side is irrelevant to k. (25), (26), and (27) together complete the proof. □

B. Proof of Proposition 2

We first prove sequence (20) is non-decreasing in mutual information. Let $P_{\mathcal{K}}(x_{m_{\mathcal{K}}}) = \prod_{q\in\mathcal{K}} P_q(x_{m_q})$ and $P'_{\mathcal{K}}(x_{m_{\mathcal{K}}}) = P'_k(x_{m_k}) \prod_{q\in\mathcal{K}\setminus\{k\}} P_q(x_{m_q})$ be two probability distributions with potentially different marginal for tag $k \in \mathcal{K}$ at state $m_k \in \mathcal{M}$, and define an intermediate function $J(P_{\mathcal{K}}(x_{m_{\mathcal{K}}}),P'_{\mathcal{K}}(x_{m_{\mathcal{K}}}))$ as (28). It is straightforward to verify $J\left(P_{\mathcal{K}}(x_{m_{\mathcal{K}}}),P_{\mathcal{K}}(x_{m_{\mathcal{K}}})\right) = I(x_{\mathcal{K}};\, \hat{x}_{\mathcal{K}},\, \boldsymbol{y})$ and $J\left(P_{\mathcal{K}}(x_{m_{\mathcal{K}}}),P'_{\mathcal{K}}(x_{m_{\mathcal{K}}})\right)$ is a concave function for a fixed $P'_{\mathcal{K}}(x_{m_{\mathcal{K}}})$. By choosing $\nabla_{P_k^\star(x_{m_k})} J(P_{\mathcal{K}}(x_{m_{\mathcal{K}}}),P'_{\mathcal{K}}(x_{m_{\mathcal{K}}})) = 0$, we have

$$S'_k(x_{m_k}) - S'_k(x_{i_k}) + (1-\rho)\log\frac{P_k(x_{i_k})}{P_k^\star(x_{m_k})} = 0, \tag{29}$$

where $i_k \neq m_k$ is the reference state and

$$S'_k(x_{m_k}) \triangleq I'_k(x_{m_k};\hat{x}_{\mathcal{K}},\boldsymbol{y}) + (1-\rho) \sum_{m_{\mathcal{K}\setminus\{k\}}} P_{\mathcal{K}\setminus\{k\}}(x_{m_{\mathcal{K}\setminus\{k\}}}) \times \sum_{m'_{\mathcal{K}}} P(\hat{x}_{m'_{\mathcal{K}}} \,|\, x_{m_{\mathcal{K}}}) \log P'_{\mathcal{K}}(x_{m_{\mathcal{K}}}). \tag{30}$$

Evidently, $\forall m_k \neq i_k$, (29) boils down to

$$P_k^\star(x_{m_k}) = \frac{P'_k(x_{m_k}) \exp\left(\frac{\rho}{1-\rho} I'_k(x_{m_k};\hat{x}_{\mathcal{K}},\boldsymbol{y})\right)}{\sum_{m'_k} P'_k(x_{m'_k}) \exp\left(\frac{\rho}{1-\rho} I'_k(x_{m'_k};\hat{x}_{\mathcal{K}},\boldsymbol{y})\right)}. \tag{31}$$

Although it seems $P_k(x_{i_k}) = 1 - \sum_{m_k \neq i_k} P_k^\star(x_{m_k})$ has no optimality guarantee, we can verify that $P_k(x_{i_k})$ has exactly the same form as (31). It implies the selection of reference state does not matter and (31) is indeed optimal $\forall m_k \in \mathcal{M}$. Therefore, for a fixed $P'_{\mathcal{K}}(x_{m_{\mathcal{K}}})$, choosing $P_k(x_{m_k})$ by (31) ensures

$$J(P_{\mathcal{K}}(x_{m_{\mathcal{K}}}),P'_{\mathcal{K}}(x_{m_{\mathcal{K}}})) \ge I'(x_{\mathcal{K}};\hat{x}_{\mathcal{K}},\boldsymbol{y}). \tag{32}$$

On the other hand, (31) also guarantees

$$\begin{aligned}
\Delta &\triangleq I(x_{\mathcal{K}};\hat{x}_{\mathcal{K}},\boldsymbol{y}) - J(P_{\mathcal{K}}(x_{m_{\mathcal{K}}}),P'_{\mathcal{K}}(x_{m_{\mathcal{K}}})) && \text{(33a)}\\
&= (1-\rho) \sum_{m_k} \frac{P'_k(x_{m_k}) f'_k(x_{m_k};\hat{x}_{\mathcal{K}},\boldsymbol{y})}{\sum_{m'_k} P'_k(x_{m'_k}) f'_k(x_{m'_k};\hat{x}_{\mathcal{K}},\boldsymbol{y})} \sum_{m''_{\mathcal{K}}} P(\hat{x}_{m''_{\mathcal{K}}} \,|\, x_{m_k}) \\
&\quad \times \log \frac{\sum_{m'_k} P'_k(x_{m'_k}) P(\hat{x}_{m''_{\mathcal{K}}} \,|\, x_{m'_k}) f'_k(x_{m_k};\hat{x}_{\mathcal{K}},\boldsymbol{y})}{\sum_{m'_k} P'_k(x_{m'_k}) P(\hat{x}_{m''_{\mathcal{K}}} \,|\, x_{m'_k}) f'_k(x_{m'_k};\hat{x}_{\mathcal{K}},\boldsymbol{y})} && \text{(33b)}\\
&\ge (1-\rho) \sum_{m_k} \frac{P'_k(x_{m_k}) f'_k(x_{m_k};\hat{x}_{\mathcal{K}},\boldsymbol{y})}{\sum_{m'_k} P'_k(x_{m'_k}) f'_k(x_{m'_k};\hat{x}_{\mathcal{K}},\boldsymbol{y})} \sum_{m''_{\mathcal{K}}} P(\hat{x}_{m''_{\mathcal{K}}} \,|\, x_{m_k}) \\
&\quad \times \left(1 - \frac{\sum_{m'_k} P'_k(x_{m'_k}) P(\hat{x}_{m''_{\mathcal{K}}} \,|\, x_{m'_k}) f'_k(x_{m'_k};\hat{x}_{\mathcal{K}},\boldsymbol{y})}{\sum_{m'_k} P'_k(x_{m'_k}) P(\hat{x}_{m''_{\mathcal{K}}} \,|\, x_{m'_k}) f'_k(x_{m_k};\hat{x}_{\mathcal{K}},\boldsymbol{y})}\right) && \text{(33c)}\\
&= 0, && \text{(33d)}
\end{aligned}$$

where $f'_k(x_{m_k};\hat{x}_{\mathcal{K}},\boldsymbol{y}) \triangleq \exp\left(\frac{\rho}{1-\rho} I'_k(x_{m_k};\hat{x}_{\mathcal{K}},\boldsymbol{y})\right)$ and the equality holds if and only if (31) converges. (32) and (33) together imply $I(x_{\mathcal{K}};\hat{x}_{\mathcal{K}},\boldsymbol{y}) \ge I'(x_{\mathcal{K}};\hat{x}_{\mathcal{K}},\boldsymbol{y})$. Since mutual information is bounded above, we conclude the sequence (20) is non-decreasing and convergent in mutual information.

Next, we prove that any converging point of sequence (20), denoted as $P_k^\star(x_{m_k})$, fulfills KKT conditions (19). To see this, consider $P_k^{(0)}(x_{m_k}) > 0$ and define

$$D_k^{(r)}(x_{m_k}) \triangleq \frac{P_k^{(r+1)}(x_{m_k})}{P_k^{(r)}(x_{m_k})} = \frac{f_k^{(r)}(x_{m_k};\hat{x}_{\mathcal{K}},\boldsymbol{y})}{\sum_{m'_k} P_k^{(r)}(x_{m'_k}) f_k^{(r)}(x_{m'_k};\hat{x}_{\mathcal{K}},\boldsymbol{y})}. \tag{34}$$

As sequence (20) is convergent, any state with $P_k^\star(x_{m_k}) > 0$ need to satisfy $D_k^\star(x_{m_k}) \triangleq \lim_{r\to\infty} D_k^{(r)}(x_{m_k}) = 1$, namely

$$I_k^\star(x_{m_k};\hat{x}_{\mathcal{K}},\boldsymbol{y}) = \frac{1-\rho}{\rho} \log \sum_{m'_k} P_k^\star(x_{m'_k}) f_k^\star(x_{m'_k};\hat{x}_{\mathcal{K}},\boldsymbol{y}), \tag{35}$$

which is reminiscent of (25a) (and hence (19a)). That is to say, given $P_k^{(0)}(x_{m_k}) > 0$, any converging point with $P_k^\star(x_{m_k}) > 0$ must satisfy (19a). On the other hand, we assume $P_k^\star(x_{m_k})$ does not satisfy (19b), such that for any state with $P_k^\star(x_{m_k}) = 0$,

$$I_k^\star(x_{m_k};\hat{x}_{\mathcal{K}},\boldsymbol{y}) > I^\star(x_{\mathcal{K}};\hat{x}_{\mathcal{K}},\boldsymbol{y}) = \sum_{m'_k} P_k^\star(x_{m'_k}) I_k^\star(x_{m'_k};\hat{x}_{\mathcal{K}},\boldsymbol{y}), \tag{36}$$

where the equality inherits from (16). Since the exponential function is monotonically increasing, we have $f_k^\star(x_{m_k};\hat{x}_{\mathcal{K}},\boldsymbol{y}) >$

$$\begin{aligned}
J(P_{\mathcal{K}}(x_{m_{\mathcal{K}}}),P'_{\mathcal{K}}(x_{m_{\mathcal{K}}})) &\triangleq \rho \sum_{m_{\mathcal{K}}} P_{\mathcal{K}}(x_{m_{\mathcal{K}}}) \log_2\left(1 + \frac{|\boldsymbol{h}_{\mathrm{E}}^H(x_{m_{\mathcal{K}}})\boldsymbol{w}|^2}{\sigma_w^2}\right) \\
&\quad + (1-\rho) \sum_{m_{\mathcal{K}}} P_{\mathcal{K}}(x_{m_{\mathcal{K}}}) \sum_{m'_{\mathcal{K}}} P(\hat{x}_{m'_{\mathcal{K}}} \,|\, x_{m_{\mathcal{K}}}) \log \frac{P(\hat{x}_{m'_{\mathcal{K}}} \,|\, x_{m_{\mathcal{K}}}) P'_{\mathcal{K}}(x_{m_{\mathcal{K}}})}{P'(\hat{x}_{m'_{\mathcal{K}}}) P_{\mathcal{K}}(x_{m_{\mathcal{K}}})}.
\end{aligned} \tag{28}$$

$\sum_{m'_k} P_k^\star(x_{m'_k}) f_k^\star(x_{m'_k};\hat{x}_\mathcal{K},\boldsymbol{y})$ and $D_k^\star(x_{m_k})>1$. Considering $P_k^{(0)}(x_{m_k})>0$ and $P_k^\star(x_{m_k})=0$, it contradicts with

$$P_k^{(r)}(x_{m_k}) = P_k^{(0)}(x_{m_k}) \prod_{n=1}^{r} D_k^{(n)}(x_{m_k}). \tag{37}$$

Therefore, given $P_k^{(0)}(x_{m_k})>0$, any converging point with $P_k^\star(x_{m_k})=0$ must satisfy (19b). This completes the proof. □

C. Proof of Proposition 3

Since L input letters are with non-zero probability and $x\to z\to\hat{x}$ formulates a Markov chain, we need L non-empty decision regions and at least $L+1$ distinct thresholds (including 0 and ∞) to minimize the distortion between source and decision. On the other hand, the optimal decision regions are apparently empty for those unused letters.

Suppose the optimal number of thresholds is $S+1$ where $S\geq L$. Let $\boldsymbol{t}\triangleq[t_0,...,t_S]^T\in\mathbb{R}_+^{(S+1)\times 1}$ be the optimal threshold vector where $t_{s-1}<t_s$, $\forall s\in\mathcal{S}\triangleq\{1,...,S\}$. Since the optimal decision region for any letter may consist of multiple partitions, without loss of generality, we assume the mapping from threshold vector to decision region $l'\in\mathcal{L}\triangleq\{1,...,L\}$ is given by $\mathcal{R}_{l'}=\bigcup_{s\equiv l' \pmod L}[t_{s-1},t_s)$. [5]he proof holds for any valid mapping from threshold vector to decision regions, and we consider this specific case for the ease of presentation. The threshold optimization problem is

$$\max_{\boldsymbol{t}} \quad I_\mathrm{B}(x;\hat{x}) \tag{38a}$$

$$\text{s.t.} \quad t_{s-1}<t_s, \quad \forall s\in\mathcal{S}. \tag{38b}$$

Problem (38) is intricate due to the strict inequality constraint (38b). Following [46], we first relax it to the convex counterpart, then discard the solutions that violate any original constraint. The Lagrangian function for the relaxed problem is

$$L=-I_\mathrm{B}(x;\hat{x})+\sum_{s\in\mathcal{S}}\mu_s(t_{s-1}-t_s), \tag{39}$$

where μ_s is the Lagrange multiplier associated with the non-strict version of (38b). The KKT conditions on the optimal primal and dual solutions are, $\forall s\in\mathcal{S}$,

$$-\nabla_{t_s^\star} I_\mathrm{B}^\star(x;\hat{x})+\mu_{s-1}^\star-\mu_s^\star=0, \tag{40a}$$

$$\mu_s^\star\geq 0, \tag{40b}$$

$$\mu_s^\star(t_{s-1}^\star-t_s^\star)=0. \tag{40c}$$

Due to the strict inequality constraint (38b), conditions (40b) and (40c) together imply $\mu_s^\star=0$, $\forall s\in\mathcal{S}$. Besides, it is trivial to conclude $t_0^\star=0$ for energy-based detection. As such, the necessary optimality conditions for problem (38), $\forall s\in\mathcal{S}$,

$$\nabla_{t_s^\star} I_\mathrm{B}^\star(x;\hat{x})=0, \tag{41}$$

which can be explicitly written as, $\forall s\equiv l' \pmod L$,

$$\sum_l P(x_l)\frac{(t_s^\star)^{N-1}e^{-t_s^\star/\sigma_l^2}}{\sigma_l^{2N}(N-1)!}\log\frac{P(x_l\,|\,\hat{x}_{l'+1})}{P(x_l\,|\,\hat{x}_{l'})}=0, \tag{42}$$

[5]T

According to [44], the optimal backward channel quantizer is convex and separates each pair of posterior distribution by a hyperplane. It implies, for a given output letter l', the sequence $\{\log P(x_l\,|\,\hat{x}_{l'+1})/P(x_l\,|\,\hat{x}_{l'})\}_{l\in\mathcal{L}}$ changes sign exactly once. We notice the left-hand side of (42) is a generalized Dirichlet polynomial, and by Descartes' rule of signs [47], has at most one positive solution. In other words, starting from $t_0^\star$, each optimal decision region requires at most one additional distinct threshold, and we have $S\leq L$. Therefore, we conclude $S=L$ and the proof is completed. □

REFERENCES

[1] V. Liu, A. Parks, V. Talla, S. Gollakota, D. Wetherall, and J. R. Smith, "Ambient backscatter: Wireless communication out of thin air," *ACM SIGCOMM Computer Communication Review*, vol. 43, pp. 39–50, 9 2013. [Online]. Available: https://dl.acm.org/doi/10.1145/2534169.2486015

[2] G. Yang, Y.-C. C. Liang, R. Zhang, and Y. Pei, "Modulation in the air: Backscatter communication over ambient ofdm carrier," *IEEE Transactions on Communications*, vol. 66, pp. 1219–1233, 3 2018. [Online]. Available: http://ieeexplore.ieee.org/document/8103807/

[3] G. Yang, Q. Zhang, and Y.-C. Liang, "Cooperative ambient backscatter communications for green internet-of-things," *IEEE Internet of Things Journal*, vol. 5, pp. 1116–1130, 4 2018. [Online]. Available: https://ieeexplore.ieee.org/document/8274950/

[4] Y.-C. Liang, Q. Zhang, E. G. Larsson, and G. Y. Li, "Symbiotic radio: Cognitive backscattering communications for future wireless networks," *IEEE Transactions on Cognitive Communications and Networking*, vol. 6, pp. 1242–1255, 12 2020. [Online]. Available: https://ieeexplore.ieee.org/document/9193946/

[5] H. Guo, Y.-C. Liang, R. Long, and Q. Zhang, "Cooperative ambient backscatter system: A symbiotic radio paradigm for passive iot," *IEEE Wireless Communications Letters*, vol. 8, pp. 1191–1194, 8 2019. [Online]. Available: https://ieeexplore.ieee.org/document/8692391/

[6] H. Ding, D. B. da Costa, and J. Ge, "Outage analysis for cooperative ambient backscatter systems," *IEEE Wireless Communications Letters*, vol. 9, pp. 601–605, 5 2020. [Online]. Available: https://ieeexplore.ieee.org/document/8941106/

[7] R. Long, Y.-C. Liang, H. Guo, G. Yang, and R. Zhang, "Symbiotic radio: A new communication paradigm for passive internet of things," *IEEE Internet of Things Journal*, vol. 7, pp. 1350–1363, 2 2020. [Online]. Available: https://ieeexplore.ieee.org/document/8907447/

[8] S. Zhou, W. Xu, K. Wang, C. Pan, M.-S. Alouini, and A. Nallanathan, "Ergodic rate analysis of cooperative ambient backscatter communication," *IEEE Wireless Communications Letters*, vol. 8, pp. 1679–1682, 12 2019. [Online]. Available: https://ieeexplore.ieee.org/document/8807353/

[9] T. Wu, M. Jiang, Q. Zhang, Q. Li, and J. Qin, "Beamforming design in multiple-input-multiple-output symbiotic radio backscatter systems," *IEEE Communications Letters*, vol. 25, pp. 1949–1953, 6 2021. [Online]. Available: https://ieeexplore.ieee.org/document/9358202/

[10] J. Xu, Z. Dai, and Y. Zeng, "Enabling full mutualism for symbiotic radio with massive backscatter devices," *arXiv:2106.05789*, 6 2021. [Online]. Available: http://arxiv.org/abs/2106.05789

[11] H. Yang, Y. Ye, K. Liang, and X. Chu, "Energy efficiency maximization for symbiotic radio networks with multiple backscatter devices," *IEEE Open Journal of the Communications Society*, vol. 2, pp. 1431–1444, 2021. [Online]. Available: https://ieeexplore.ieee.org/document/9461158/

[12] S. Han, Y.-C. Liang, and G. Sun, "The design and optimization of random code assisted multi-bd symbiotic radio system," *IEEE Transactions on Wireless Communications*, vol. 20, pp. 5159–5170, 8 2021. [Online]. Available: https://ieeexplore.ieee.org/document/9382925/

[13] Q. Wu and R. Zhang, "Intelligent reflecting surface enhanced wireless network: Joint active and passive beamforming design," vol. 18. IEEE, 12 2018, pp. 1–6. [Online]. Available: https://ieeexplore.ieee.org/document/8647620/

[14] S. Zhang and R. Zhang, "Capacity characterization for intelligent reflecting surface aided mimo communication," *IEEE Journal on Selected Areas in Communications*, vol. 38, pp. 1823–1838, 8 2020. [Online]. Available: https://ieeexplore.ieee.org/document/9110912/

[15] S. Lin, B. Zheng, F. Chen, and R. Zhang, "Intelligent reflecting surface-aided spectrum sensing for cognitive radio," *IEEE Wireless Communications Letters*, vol. 11, pp. 928–932, 5 2022.

[16] Y. Liu, Y. Zhang, X. Zhao, S. Geng, P. Qin, and Z. Zhou, "Dynamic-controlled ris assisted multi-user miso downlink system: Joint beamforming design," *IEEE Transactions on Green Communications and Networking*, vol. 6, pp. 1069–1081, 6 2022.

[17] Z. Feng, B. Clerckx, and Y. Zhao, "Waveform and beamforming design for intelligent reflecting surface aided wireless power transfer: Single-user and multi-user solutions," *IEEE Transactions on Wireless Communications*, 2022.

[18] Y. Zhao, B. Clerckx, and Z. Feng, "Irs-aided swipt: Joint waveform, active and passive beamforming design under nonlinear harvester model," *IEEE Transactions on Communications*, vol. 70, pp. 1345–1359, 2022.

[19] Y. Yang, S. Zhang, and R. Zhang, "Irs-enhanced ofdma: Joint resource allocation and passive beamforming optimization," *IEEE Wireless Communications Letters*, vol. 9, pp. 760–764, 6 2020. [Online]. Available: https://ieeexplore.ieee.org/document/8964457/

[20] Q. Wu, X. Zhou, W. Chen, J. Li, and X. Zhang, "Irs-aided wpcns: A new optimization framework for dynamic irs beamforming," *IEEE Transactions on Wireless Communications*, pp. 1–1, 12 2021.

[21] M. Hua and Q. Wu, "Joint dynamic passive beamforming and resource allocation for irs-aided full-duplex wpcn," *IEEE Transactions on Wireless Communications*, pp. 1–1, 12 2021.

[22] C. Qiu, Q. Wu, M. Hua, X. guan, and Y. Wu, "Achieving multi-beam gain in intelligent reflecting surface assisted wireless energy transfer," *arXiv:2205.08893*, 5 2022. [Online]. Available: http://arxiv.org/abs/2205.08893

[23] H. Chen, G. Yang, and Y.-C. Liang, "Joint active and passive beamforming for reconfigurable intelligent surface enhanced symbiotic radio system," *IEEE Wireless Communications Letters*, vol. 10, pp. 1056–1060, 5 2021. [Online]. Available: https://ieeexplore.ieee.org/document/9345739/

[24] Q. Zhang, Y.-C. Liang, and H. V. Poor, "Reconfigurable intelligent surface assisted mimo symbiotic radio networks," *IEEE Transactions on Communications*, vol. 69, pp. 4832–4846, 7 2021. [Online]. Available: https://ieeexplore.ieee.org/document/9391685/

[25] R. Karasik, O. Simeone, M. D. Renzo, and S. S. Shitz, "Beyond max-snr: Joint encoding for reconfigurable intelligent surfaces," vol. 2020-June. IEEE, 6 2020, pp. 2965–2970. [Online]. Available: https://ieeexplore.ieee.org/document/9174060/

[26] X. Xu, Y.-C. Liang, G. Yang, and L. Zhao, "Reconfigurable intelligent surface empowered symbiotic radio over broadcasting signals," vol. 2020-Janua. IEEE, 12 2020, pp. 1–6. [Online]. Available: https://ieeexplore.ieee.org/document/9348236/

[27] M. Hua, Q. Wu, L. Yang, R. Schober, and H. V. Poor, "A novel wireless communication paradigm for intelligent reflecting surface based symbiotic radio systems," *IEEE Transactions on Signal Processing*, vol. 70, pp. 550–565, 4 2022. [Online]. Available: http://arxiv.org/abs/2104.09161https://ieeexplore.ieee.org/document/9652042/

[28] S. Hu, C. Liu, Z. Wei, Y. Cai, D. W. K. Ng, and J. Yuan, "Beamforming design for intelligent reflecting surface-enhanced symbiotic radio systems," *arxiv:2110.10316*, 10 2021. [Online]. Available: http://arxiv.org/abs/2110.10316

[29] Y. Huang, A. Alieldin, and C. Song, "Equivalent circuits and analysis of a generalized antenna system," *IEEE Antennas and Propagation Magazine*, vol. 63, pp. 53–62, 4 2021. [Online]. Available: https://ieeexplore.ieee.org/document/9392844/

[30] D. Dobkin, *The RF in RFID: Passive UHF RFID in Practice*. Newnes, 11 2012. [Online]. Available: https://www.elsevier.com/books/the-rf-in-rfid/dobkin/978-0-12-394583-9

[31] J. Kim and B. Clerckx, "Wireless information and power transfer for iot: Pulse position modulation, integrated receiver, and experimental validation," *arXiv:2104.08404*, pp. 1–15, 4 2021. [Online]. Available: http://arxiv.org/abs/2104.08404

[32] R. Hansen, "Relationships between antennas as scatterers and as radiators," *Proceedings of the IEEE*, vol. 77, pp. 659–662, 5 1989. [Online]. Available: http://ieeexplore.ieee.org/document/32056/

[33] C. Boyer and S. Roy, "Backscatter communication and rfid: Coding, energy, and mimo analysis," *IEEE Transactions on Communications*, vol. 62, pp. 770–785, 3 2014. [Online]. Available: http://ieeexplore.ieee.org/document/6685977/

[34] ——, "Coded qam backscatter modulation for rfid," *IEEE Transactions on Communications*, vol. 60, pp. 1925–1934, 7 2012. [Online]. Available: http://ieeexplore.ieee.org/document/6202629/

[35] Q. Wu, S. Zhang, B. Zheng, C. You, and R. Zhang, "Intelligent reflecting surface-aided wireless communications: A tutorial," *IEEE Transactions on Communications*, vol. 69, pp. 3313–3351, 5 2021. [Online]. Available: https://ieeexplore.ieee.org/document/9326394/

[36] S. J. Thomas, E. Wheeler, J. Teizer, and M. S. Reynolds, "Quadrature amplitude modulated backscatter in passive and semipassive uhf rfid systems," *IEEE Transactions on Microwave Theory and Techniques*, vol. 60, pp. 1175–1182, 4 2012. [Online]. Available: http://ieeexplore.ieee.org/document/6153042/

[37] D. Bharadia, K. R. Joshi, M. Kotaru, and S. Katti, "Backfi: High throughput wifi backscatter," vol. 45. ACM, 8 2015, pp. 283–296. [Online]. Available: https://dl.acm.org/doi/10.1145/2785956.2787490

[38] G. Yang, C. K. Ho, and Y. L. Guan, "Multi-antenna wireless energy transfer for backscatter communication systems," *IEEE Journal on Selected Areas in Communications*, vol. 33, pp. 2974–2987, 12 2015. [Online]. Available: http://ieeexplore.ieee.org/document/7274644/

[39] H. Guo, Q. Zhang, S. Xiao, and Y.-C. Liang, "Exploiting multiple antennas for cognitive ambient backscatter communication," *IEEE Internet of Things Journal*, vol. 6, pp. 765–775, 2 2019. [Online]. Available: https://ieeexplore.ieee.org/document/8411483/

[40] Q. Wu and R. Zhang, "Intelligent reflecting surface enhanced wireless network via joint active and passive beamforming," *IEEE Transactions on Wireless Communications*, vol. 18, pp. 5394–5409, 11 2019. [Online]. Available: https://ieeexplore.ieee.org/document/8811733/

[41] J. Buhler and G. Wunder, "A note on capacity computation for the discrete multiple access channel," *IEEE Transactions on Information Theory*, vol. 57, pp. 1906–1910, 4 2011. [Online]. Available: https://ieeexplore.ieee.org/document/5730559/

[42] S. Arimoto, "An algorithm for computing the capacity of arbitrary discrete memoryless channels," *IEEE Transactions on Information Theory*, vol. 18, pp. 14–20, 1 1972. [Online]. Available: http://ieeexplore.ieee.org/document/1054753/

[43] R. E. Blahut, "Computation of channel capacity and rate-distortion functions," *IEEE Transactions on Information Theory*, vol. 18, pp. 460–473, 7 1972. [Online]. Available: http://ieeexplore.ieee.org/document/1054855/

[44] X. He, K. Cai, W. Song, and Z. Mei, "Dynamic programming for sequential deterministic quantization of discrete memoryless channels," *IEEE Transactions on Communications*, vol. 69, pp. 3638–3651, 6 2021. [Online]. Available: https://ieeexplore.ieee.org/document/9366549/

[45] T. Nguyen and T. Nguyen, "On thresholding quantizer design for mutual information maximization: Optimal structures and algorithms," vol. 2020-May. IEEE, 5 2020, pp. 1–5. [Online]. Available: https://ieeexplore.ieee.org/document/9128966/

[46] T. D. Nguyen and T. Nguyen, "On binary quantizer for maximizing mutual information," *IEEE Transactions on Communications*, vol. 68, pp. 5435–5445, 9 2020. [Online]. Available: https://ieeexplore.ieee.org/document/9118952/

[47] G. J. O. Jameson, "Counting zeros of generalised polynomials: Descartes' rule of signs and laguerre's extensions," *The Mathematical Gazette*, vol. 90, pp. 223–234, 7 2006. [Online]. Available: https://www.cambridge.org/core/product/identifier/S0025557200179628/type/journal_article